Thermo-optical coupling applied to high luminance LED used in automotive front lighting

Clément Rongier, Rémi Gilblas, N. Rasoldier, Fabrice Schmidt, Yannick Le Maoult

Thermo-optical coupling applied to high luminance LED used in automotive front lighting

C. Rongier [a], R. Gilblas [a,*], N. Rasoldier [b], F. Schmidt [a], Y. Le Maoult [a]

[a] *IMT Mines Albi, Institut Clément Ader, Campus Jarlard, Albi Cedex 09, 81013, France*

[b] *Valeo Lighting Systems, 34 rue Saint André, Bobigny, 93000, France*

Automotive front lighting evolved towards high definition beams. To create such function, up to several light source per square millimeters are involved. The current trend tends to replace multiple LED designs with only one high luminance LED. The 10W-optical power emitted by this optoelectronic source induces high energy density that requires to be thermally managed. Moreover, when this LED is integrated within its optical system, the radiation concentration can lead to the system self-heating, leading to early damage or failure. The strategy adopted in this paper to avoid the component failure consists in developing an accurate and robust multi-physics simulation to predict heat transfer in a LED lighting system. In this paper, the validation of a high luminance LED thermo-optical coupling model is achieved by comparing numerical simulations with experimental results. The full optical characterization of LED has been performed to build its opto-thermal model. Then, an experimental set-up has been designed and consists in positioning a black plate in front of the LED, to capture its self-heating induced by light energy absorption using infrared thermography. The agreement between thermo-optical simulation and IR thermography is fair, which reinforces the use of the model with an error lower than 10%.

1. Introduction

For a couple of years, automotive lighting technologies evolved towards new functionalities such as glare free beams [1]. To provide high definitions beams, conventional LEDs design is replaced by a new optoelectronic component [2]. Such light sources emit an optical power up to 10 W, inducing high densities of energy which require to be thermally controlled. Indeed, to ensure both optical performance and reliability, the thermal management of high-powered LED is of prime interest [3]. One of the main issues in the automotive lighting application is the high density energy within the optical system. According to their efficiency, the luminous flux emitted by LEDs can be absorbed by optical systems and converted into heat, which is responsible for the lighting system temperature rise. In this context, robust and accurate simulation models must be developed to predict how the luminous energy emitted by the LED interacts with its environment, *i.e.* coupling between the three heat transfer modes (conduction, convection and radiation). Moreover, due to the complex geometry found in automotive lighting, a good computation time–solution accuracy must be ensured.

Based on the use of the CFD code ADINA-F, a coupling between specular radiation and fluid flow analysis using ray-tracing method was studied numerically by Moore et al. [4]. This was applied to automotive lamp thermal analysis to predict temperature increase of lamps induced by radiation and natural convection heating. Filipuzzi et al. [5] have coupled a ray-tracing method to the commercial CFD software Ansys CFX to analyze the thermal behavior of bulb and LED lamps. A multi-bands approach was considered to take into account the spectral properties. More recently, Dauphin et al. [6] have proposed a thermal simulation method, in which heat transfer are solved in an decoupled manner. The radiatif heat source was determined using a Monte Carlo method and was applied as a boundary condition in the CFD simulation. Such an approach was further investigated to model radiative heat transfer within a semi-crystalline thermoplastics [7]. The study was carried out using an in-house radiation heat transfer algorithm and the commercial software COMSOL Multiphysics. An iterative process was performed using Matlab: the radiation source was calculated and then implemented in the CFD software. An alternative of the previous method consists in solving the three heat transfer equations in a coupled manner. Barreto et al. [8] have analyzed the thermal performance of a porous volumetric receiver element coupled to solar concentration system. The fluid flow and heat transfer were modeled through volume averaged mass, momentum and energy conservation equations. An in-house algorithm based on the Monte Carlo ray-tracing method was developed and coupled to the CFD mesh to take into account the solar radiation.

To accurately predict the self-heating of the optical system induced by light absorption, it is necessary to develop a model that takes this phenomenon into account during the thermal simulation. To model the optical behavior of a light-emitting diode, the Monte Carlo ray-tracing (MCRT) technique is used. Ting and McGill [9] have employed

a MCRT simulation to model the light emission of a LED lamp. Light was modeled by photons emitted in an isotropic spatial pattern and obey to the geometrical optics laws (*i.e.* taking into account reflection and refraction). The LED radiation patterns need to be well modeled to reproduce the emitting behavior of the component. Thus, Moreno and Sun [10] have developed a mathematical model to accurately account for several LEDs radiation patterns. Such a model was then compared to supplier data and predicted the angular distribution of optoelectronic components. Then, Liu et al. [11] proposed an accurate optical modeling of a blue light-emitting diode. To do so, the optical characterization of the blue chip has been performed, based on modeling and from literature data. Then, a MCRT simulation was conducted, in which photons are randomly emitted from the LED active region. The radiation pattern was obtained from simulation based on the angular dependence of photon and was compared with experiments performed with goniophotometer. Lan et al. [12] employed MCRT simulations to analyze the light extraction of several LEDs at a central wavelength (*i.e.* for a emission peak obtained at a fixed wavelength). These studies shows the limitation of MCRT simulation applied on LEDs, in which only a constant value of wavelength is considered. Therefore, in case of white LEDs, MCRT simulation must take into account the real emission spectra of LED, in which radiant energy is wavelength dependent. Based on a literature review, Hertel et al. [13] discussed different optical models to simulate the influence of solar radiation on materials involved in concentrating solar collectors. Radiation was modeled using Monte Carlo Ray-Tracing approach while optical properties in terms of absorption, transmission and reflection where incidence angle and wavelength dependent. Based on the previous discussed study, we address several ways of investigation in order to develop a coupled thermo-optic simulation of high luminance LED used in automotive lighting products.

In this paper, a novel numerical approach for high luminance LED thermo-optical analysis is proposed. The computational study was carried out using the commercial CFD software FloEFD™ based on a Finite Volume Method, in which a Ray-Tracing (RT) method was implemented to solve the radiation heat transfers. This allows to predict the thermo-optical behavior of the optoelectronic source in a coupled way. For the study, a reference analytical solution is used to validate the RT method and to study the sensitivity of the calculation to the mesh size and the number of rays. Once this method was validated, the emission model of LED was implemented in the simulation software. For this purpose, the complete optical characterization of the light source was performed by spectrophotometry and goniophotometry. In order to assess the accuracy of the coupled CFD-radiation simulation, heating experiments were performed using an opaque PTFE plate. A high luminance LED mounted on its cooling system was positioned in front of the PTFE plate and then switched on. Thus, a part of the emitted luminous energy (up to 10 W) is absorbed and induces the self-heating of plate. Finally, temperature measurement of the plate back surface were performed via IR thermography and were compared with numerical results. The outline of the paper is as follows. The validation of the RT method is carried out in Section 2. In Section 3, the complete optical characterization of high luminance LED is performed to develop the corresponding emission model. The sensitivity of the number of rays in a complex configuration is studied in Section 4. Finally, experimental and numerical results are compared.

2. Evaluation of the heat transfer simulation on a reference case

2.1. Mathematical formulation and numerical model

Thermo-optical behavior of a high luminance LED is predicted by CFD simulations coupled with radiation. The use of CFD models avoids time-consuming iterative calculation induced by numerical models [14]. Moreover, CFD model eliminates the formulation limitations and iterative calculation process of exchange coefficient from semi-empirical formulas. Hence, a 3D thermo-optical simulation of high luminance LED was conducted using FloEFD™ 2019.2.

The governing equations are discretized using the finite volume (FV) method. Following this approach, the discretization of the integral form of the conservation laws is performed. A cartesian rectangular coordinate system is used and the control volumes are rectangular parallelepipeds. All physical parameters are determined at the control volume mass center. The spatial derivatives are approximated thanks to implicit difference operators of second-order accuracy. The Ray-tracing method was implemented in the CFD software in order to numerically solve radiation heat transfers. This allows to consider both spectral properties and absorption in solids. Thus, the method is relevant to develop the LED emission model directly coupled to CFD simulation. Nevertheless, this requires to be validated by comparison with a reference solution.

A fan which rotation speed and radius are respectively 5100rpm and 22.5 mm blows air onto 22.8 mm-length and 56 mm-width fins. Assuming that air is blown in a channel which diameter is the same as the fan rotor, a Reynolds number has been calculated using Eq. (1) in order to determine whether the flow is turbulent or not at the cooling system location.

$$Re = \frac{U\,L}{\nu} \tag{1}$$

where U is the air velocity at the fan outlet, ν is the kinematic viscosity of air at 25 °C and L is the length of the fins. Using the fan characteristics, the Re number value is about 18 000. Hence, turbulent condition were accounted for the air flow at the cooling system location.

The Grashoff number on the plate surface was calculated using Eq. (2).

$$Gr = \frac{g\beta\left(T_p - T_\infty\right)L^3}{\nu^2} \tag{2}$$

where L is the plate height of 400 mm, g is the gravitational acceleration, T_p is the surface temperature of plate, T_∞ is the ambient temperature and ν is the kinematic viscosity of air. Since the work is performed at the atmospheric pressure, air is assumed as an ideal gas. Thus, the expansion coefficient β is estimated as follows:

$$\beta = 1/T_f \tag{3}$$

where T_f is the film temperature of air and was calculated using Eq. (4).

$$T_f = (T_p + T_\infty)/2 \tag{4}$$

To calculate the Gr number, the surface temperature of the plate is assumed to be uniform and equal to 60 °C. This gives a Gr value of 1.5×10^8. According to Bejan and Lage [15], the laminar to turbulent transition in natural convection along a vertical surface occurs when the Gr number is of the order of 10^9. This means that the air flow along the vertical plate stays laminar.

To conduct the three-dimensional simulation, following assumptions were made:

1. Steady-state.
2. Fluid flow is laminar in the computational domain except at the fan location.
3. The effects induced by viscous dissipation are negligible.
4. The effects induced by thermal expansion are negligible.

The governing equations for the steady-state conditions which are formulation of mass, momentum and energy conservation equation are given as follows [16].

$$\nabla \cdot (\rho \mathbf{u}) = 0 \tag{5}$$

$$\rho \mathbf{u} \cdot \nabla \mathbf{u} = -\nabla p + \nabla \cdot \left(\mu\left(\nabla \mathbf{u} + \nabla \mathbf{u}^T\right)\right) + S \tag{6}$$

$$\rho C_p\left(\mathbf{u} \cdot \nabla T\right) = \nabla \cdot (k \nabla T) - \nabla \cdot \mathbf{q}_r \tag{7}$$

where ρ is the density, u is the velocity, p is the pressure, μ is the dynamic viscosity, g is the gravitational acceleration, C_p is the thermal capacity, T is the temperature, k is the thermal conductivity and $\mathbf{q}$ is the radiative heat flux density.

The radiative heat flux density in Eq. (7) is given by:

$$\mathbf{q}_r(s) = \int_0^{\infty} \int_{\Omega=4\pi} I_\lambda(s,\Omega)\,\Omega\,d\Omega\,d\lambda \tag{8}$$

where I_λ is the spectral radiation intensity at point s along the direction Ω, I_λ is the spectral blackbody radiation intensity and κ_λ is the absorption coefficient. The variation of the spectral radiation intensity is governed by the Radiative Transfer Equation (RTE), given for a non-scattering medium as follows [17].

$$\frac{dI_\lambda}{ds} = -\kappa_\lambda I_\lambda + \kappa_\lambda I_{\lambda,b} \tag{9}$$

In FloEFD, the RTE is solved using a Monte Carlo based Ray-tracing approach. The properties of the enclosure and the laws of probability are used to simulate an interaction with a given surface/volume [16]:

1. Photon keeps its energy while passing transparent media, and undergo an exponential decrease of energy while passing through absorptive media.
2. Photon interaction with surfaces of non-transparent media is modeled accordingly to surface emissivity coefficient values (e.g. for a black body, photon is fully absorbed).
3. The reflection properties of the surface are modeled also with statistical approach, *i.e.* corresponding coefficients are treated as probability.

In FloEFD, laminar and turbulent flows are predicted with only one system of equation based on the Favre-averaged Navier–Stokes equations [16]. In case of turbulent flows, the k-ε model is used with a range of additional empirical enhancement. For instance, damping functions proposed by Lam and Bremhorst for better boundary layer profile fit have been added (the LB k-ε model) [18]. To describe the turbulent boundary layer, the Van Driest universal profiles are employed and two approaches called "Two-Scale Wall Functions" are involved to fit a fluid's boundary layer profile relative to the main flow's properties.

The computational domain was set to 1 m × 1 m × 1 m in the x–y–z directions, as shown in Fig. 1(a).

For the boundary conditions: The ambient temperature was set to 25 °C, according to laboratory room temperature. To take into account the gravitational effect, a gravitational acceleration of 9.81 m/s^2 was implemented in the negative z direction. Regarding the fluid within the computational domain (which is composed of air), the properties are temperature dependent. The convection is so modeled based on the solving of Navier–Stokes equation by the FVM method. To model the fan, the operating curve provided by the supplier and giving the flowrate as a function of the pressure difference have been imported within the CFD software. The pressure difference between the two sides of the fan allows determining the corresponding flowrate from the fan operating curve. The emissivity of heatsink was given as 0.9. Since the LED is directly stuck on the copper plate using a thermal interface, the PCB is not taken into account in the simulation. In a previous study, the LED thermal model has been validated based on the full characterization of the LED and the description of energy balance [19]. It was notably shown that the radiative contribution emitted by the P–N junction is 100 times lower than the luminous flux so it can neglected in future work. Moreover, and as shown on Fig. 1(b), the LED cooling system is composed of a copper plate, three heat pipes and a heatsink. The materials' thermal conductivity is listed in Table 1. The heat pipes used here are hollow components crossed by a heat transfer fluid. In the model, they have been approximated by high conductivity filled cylinders to simulate heat removal from the hot source (LED) to the cold one (heatsink).

About meshing, the software uses an immersed boundary Cartesian method, which generates a suitable mesh while decreasing considerably

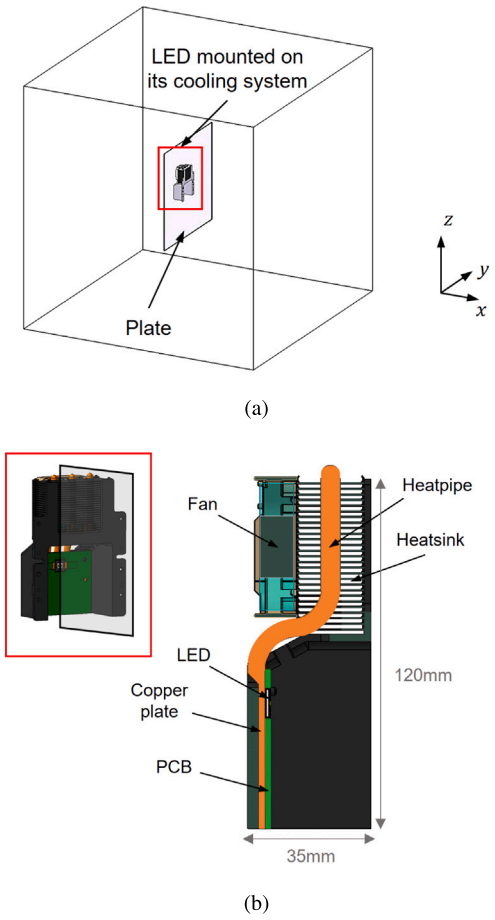

Fig. 1. Computational domain (a) and zoom on the LED system (b).

computation time [20]. An octree technique is used to refine cells and consists in subdividing the cells in two in each direction. The mesh used in this study is therefore composed of hexahedral elements. As discussed in our previous work [19], a specific refinement is applied in low thickness layer of the LED. A fluid refinement region is applied at the heatsink location to capture flow along fins. Finally, due to the location of the maximum irradiation absorption, a refinement region based on a cylinder is applied at the center of the vertical plate. The fluid region near the plate has also been refined to correctly replicate the development of the convective plume.

2.2. Validation of the radiation heat transfer resolution method

Ray-tracing (RT) method is a statistical approach used for thermal radiation analysis [21,22]. Ray-tracing allows the simulation of a wide variety of phenomena, such as reflection, refraction and absorption while taking into account the spectral dependency of optical parameters [16]. The RT method was implemented in the commercial CFD software FloEFD. To assess it, a comparison of numerical results with an analytical solution issued from view factor formulation [23] has been performed. In the present configuration, a 18 mm-squared plate is heated by a 10 W radiative source, located at a distance of 5 mm from plate. The source is modeled by a cylinder which radius and height are respectively 2.5 mm and 18 mm. The plate is the sum of the surface element dA_1 (Fig. 2). The irradiation exchanged between the radiative source and the plate is computed with RT method and view factor given

Table 1
Thermal conductivity of each material.

Component	Material	Thermal conductivity [W/m K]
LED	Phosphor converter	1.2 (equivalent)
	LED Chips	46 (equivalent)
	Solder	15 (equivalent)
	Substrate (ceramic)	170
Thermal interface	–	6.8 (equivalent)
Copper plate	Copper	400
Heat pipe	–	15000
Heatsink	Aluminum 6061	155.5
Opaque plate	PTFE	0.25

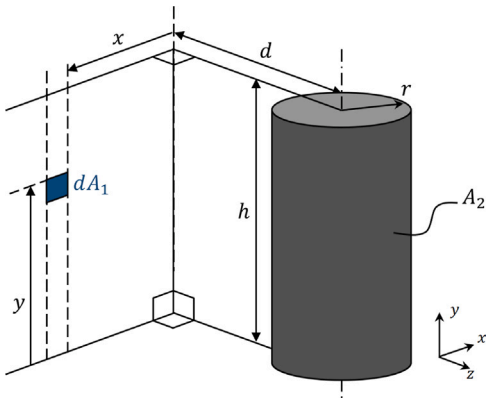

Fig. 2. Geometrical configuration for Eq. (10).

by Eq. (10), respectively. The geometrical variables (s, x, z, h) are defined on Fig. 2.

$$F_{d_1\to 2} = \frac{S}{B} - \frac{S}{2B\pi}\times \left(\begin{array}{l} \cos^{-1}\left(\frac{Y^2-B+1}{A-1}\right) + \cos^{-1}\left(\frac{C-B+1}{C+B-1}\right) \\ - Y\frac{A+1}{\sqrt{(A-1)^2+4Y^2}}\cos^{-1}\left(\frac{Y^2-B+1}{\sqrt{B}(A-1)}\right) \\ - \frac{\sqrt{C}(C+B+1)}{\sqrt{(C+B-1)^2+4C}}\cos^{-1}\left(\frac{C-B+1}{\sqrt{B}(C+B-1)}\right) \\ + H\cos^{-1}\left(\frac{1}{\sqrt{B}}\right) \end{array} \right) \quad (10)$$

where $A = X^2 + Y^2 + S^2$; $B = S^2 + X^2$; $C = (H - Y)^2$ and $S = s/r$; $X = x/r$; $Z = z/r$; $H = h/r$.

Before proceeding to numerical results and analytical solution comparison, two preliminary studies have been performed to further investigate the sensitivity of parameters that are mesh size and number of rays.

2.2.1. Mesh sensitivity

Since the current geometry is based on a 18 mm squared plate, the mesh consists of cubic elements. Table 2 regroups the characteristics of the three meshes that have been considered for this sensitivity study. A number of rays of 500 million has been considered to minimize the statistical effects induced by a low sampling. Fig. 3 proposes the visualization of mesh sensitivity on centered horizontal and vertical irradiance profiles obtained on plate.

On one hand, both profiles obtained with a coarse mesh are smooth but highlight a spatial average of irradiance fields which is induced by the weak spatial discretization. On the other hand, when the mesh becomes finer, the spatial discretization induces a harmful effect since fluctuations are noticeable which means that a strong refinement generates a high magnitude of fluctuations (which leads to increase the numerical error). To ensure a good prediction of irradiance gradients occurring at plate surface while minimizing the numerical error, a resolution/noise compromise must be chosen. Thus, the 100 × 100 mesh size is considered to investigate the influence of the number of rays.

Table 2
Mesh used for the sensitivity study.

	Mesh 1	Mesh 2	Mesh 3
Cell size [mm]	0.36	0.18	0.09
Number of elements	50 × 50	100 × 100	200 × 200

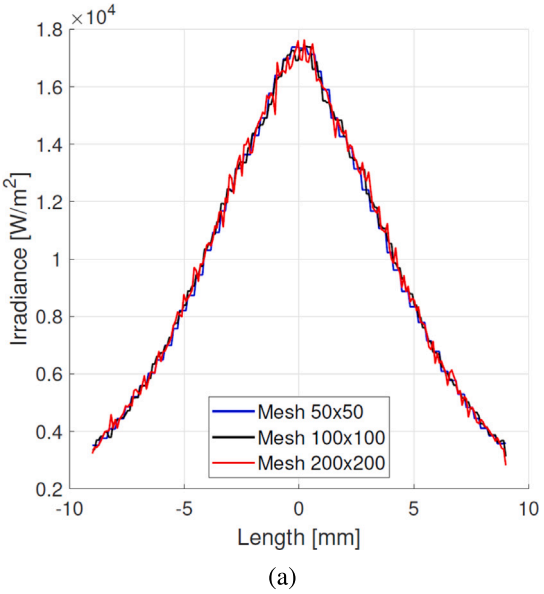

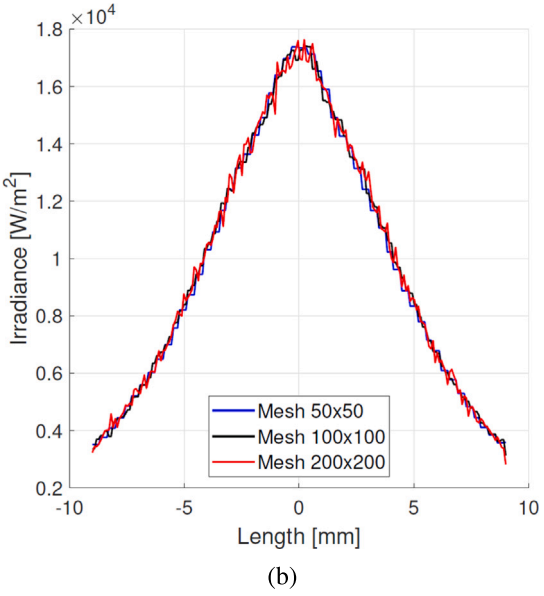

Fig. 3. Mesh sensitivity on horizontal (a) and vertical (b) irradiance profiles.

2.2.2. Rays number sensitivity

The second part of the preliminary study focuses on the sensitivity of the number of rays. For this purpose, the following numbers of rays

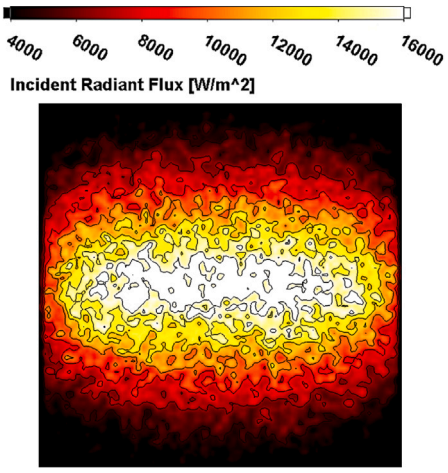

(a)

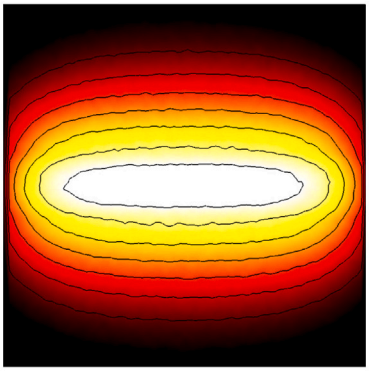

(b)

Fig. 4. Rays numbers sensitivity on irradiance field: 1 million (a) and 500 millions (b).

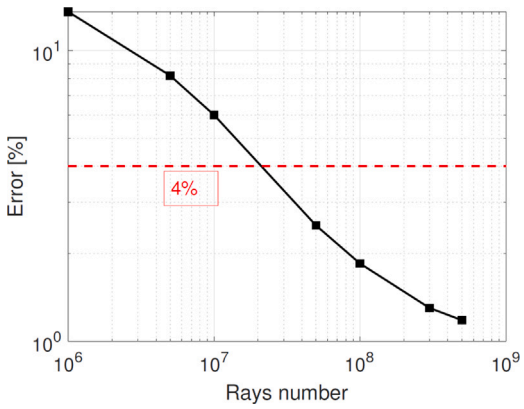

Fig. 5. Evolution of mean quadratic error versus rays numbers.

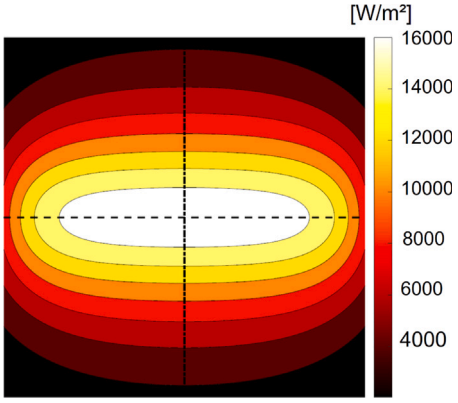

Fig. 6. Irradiance fields from analytical solution.

have been considered: 1, 5, 10, 50, 100, 300 and 500 million. Fig. 4 proposes the visualization of irradiance fields on plate obtained for 1 and 500 millions of rays, resp.

When a low number of ray is traced, the irradiance gradients occurring at plate surface are biased due to numerical noise induced by a wrong statistical sampling. When the number of rays increases, well defined gradients and smooth iso-contours are obtained. Nevertheless, few fluctuations are still noticeable. They are induced by the statistical approach of RT method but do not have a significant impact on the results. To determine the minimum number of rays required for simulation, the error between numerical and analytical solutions has been calculated on the whole plate surface S according to Eq. (11).

$$E = \sqrt{\frac{\int_S \left(I_n - I_a\right)^2 dS}{\int_S I_a^2 dS}} \times 100 \tag{11}$$

Since this preliminary study is based only on numerical analyses, a deviation of 1% was arbitrarily set for the temperature. By considering this criterion and by applying the radiative energy balance in steady state, we can deduce that this deviation on the temperature induces a 4% deviation on the irradiance. The acceptance criterion on the irradiance fields has now been determined.

Fig. 5 represents the evolution of error plotted in a log–log scale. The red line represents the acceptance criterion, as discussed above. The error decreases linearly when the number of rays increases. For 50 million rays, the acceptance criterion is reached. Moreover, when the number of rays reaches the value of 300 million, the error becomes lower than 2%.

The previous sensitivity studies allows to define the optimal mesh size and number of rays to proceed to numerical resolution of radiation using RT method. The next section proposes the comparison of results between analytical solution and numerical resolution obtained for 300 million rays.

2.2.3. Comparison between analytical solution and numerical results with 300 millions

The centered irradiance profiles in the x and y-directions (represented respectively by the dashed line and the black line on Fig. 6) have been plotted. As shown in Fig. 7, both analytical and numerical profiles follow the same trend. Nevertheless, numerical irradiance profiles highlight the presence of fluctuations, directly induced by the stochastic process used in the RT method. We can notice that the fluctuations are important in -5 mm<x,y< 5 mm, where the absorption of emitted energy by radiative source is the highest. Vertical irradiance profiles highlight more important deviation which can be explained by the gradient in the y-direction of plate.

To illustrate this purpose, Fig. 8 proposes the visualization of standard deviation between analytical solution and numerical results. Based on horizontal profiles, the relative deviations are lower than 2.5%, except close to the plate bounds. Regarding vertical profiles, deviations are lower than 6% and are obtained in -2.5 mm<y< 2.5 mm. As said previously, this is due to the irradiance gradient. Finally, in the area where irradiance is high, the error is lower than 2.5%.

According to the previous results, we can affirm that:

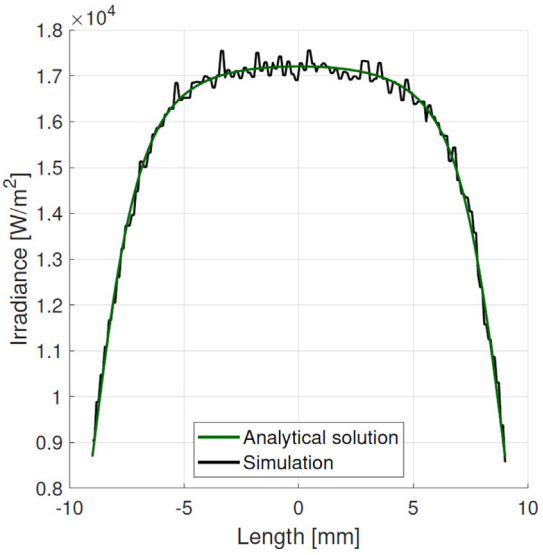

(a)

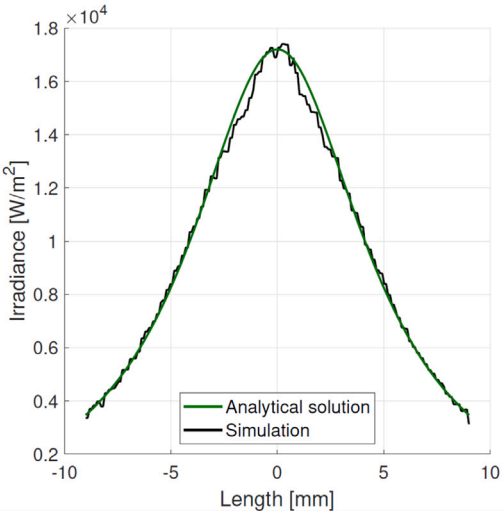

(b)

Fig. 7. Comparison of horizontal (a) and vertical (b) irradiance profiles.

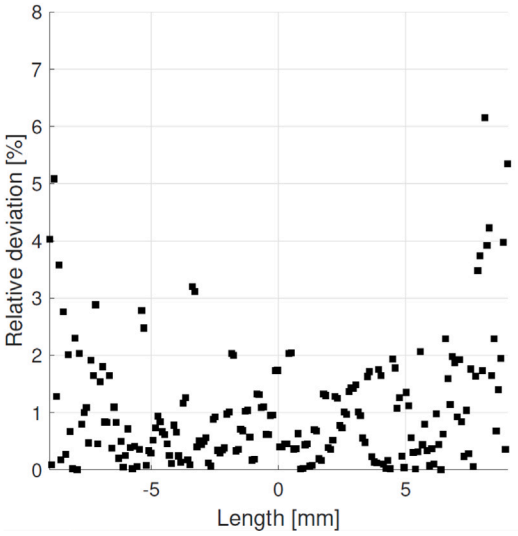

(a)

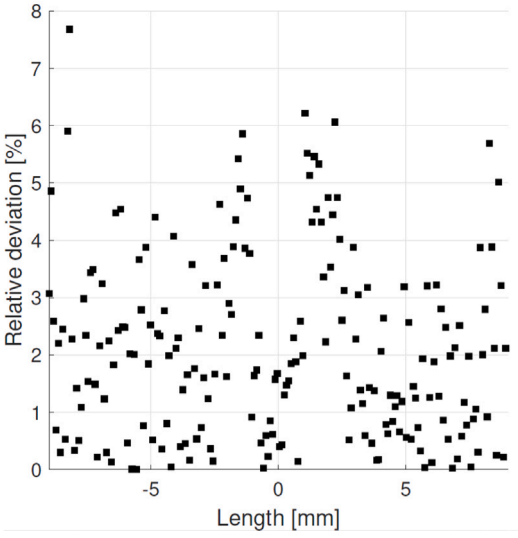

(b)

Fig. 8. Standard deviation obtained from horizontal (a) and vertical (b) irradiance profiles.

- The ray-tracing method used for solving radiation in the commercial CFD software FloEFD is validated.
- A good compromise must be ensured regarding mesh size: a coarse mesh induces a low spatial resolution while a very fine mesh induces numerical noise.
- At least 50 million rays and a 100 × 100 mesh (cell size of 0.18 mm) must be considered to ensure a quadratic error lower than 2.5%, and to respect the requirements (*i.e.* to ensure a maximum temperature deviation of 10%).

Nevertheless, the present configuration is a simple case. Thus, number of rays sensitivity in a complex geometry needs to be investigated. Before that, the next section is dedicated to the development of the high luminance LED optical model embedded in the CFD software.

3. Optical characterization and LED emission model

To develop the high luminance LED emission model embedded in the CFD software FloEFD, several parameters are required. Thus, the complete optical characterization of the optoelectronic source has been performed. To measure the spectral radiant flux emitted by the light source, a goniometer equipped with a 30-mm diameter Si photodiode detector was used to scan the LED emission over the hemisphere and the LED angular distribution (*i.e.* the so-called radiation pattern) is plotted in polar coordinates (Fig. 9(a)).

The LED radiation pattern is close to the behavior of a Lambertian source behavior, except when the angle is greater than 50°. The deviations are induced by a low signal/noise ratio of the apparatus. However, depending on the intensity level, this does not have any significant influence on the LED lambertian behavior, since at high angle, the emitted energy can be neglected.

Thanks to a spectrometer Labsphere CDS 610, the LED spectrum has been characterized, as shown in Fig. 9(b). Two emission peaks are obtained for wavelength of 450 and 555 nm. The first one is induced by the blue energy emitted by LED chips. The second extended peak is induced by absorption of blue energy occurring in the phosphor converter and re-emission of energy in the bandwidth [500–700]nm. *In fine*, high luminance LED emits white light.

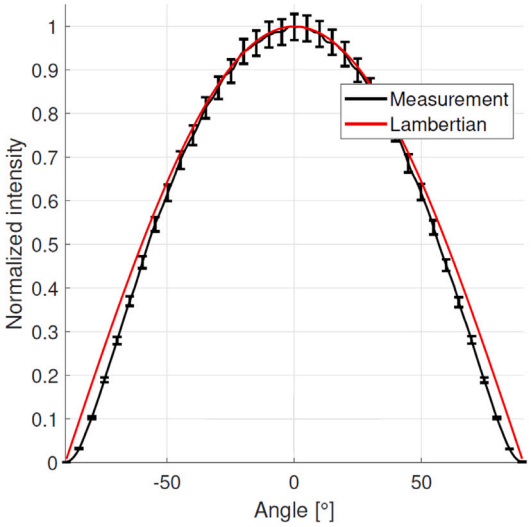

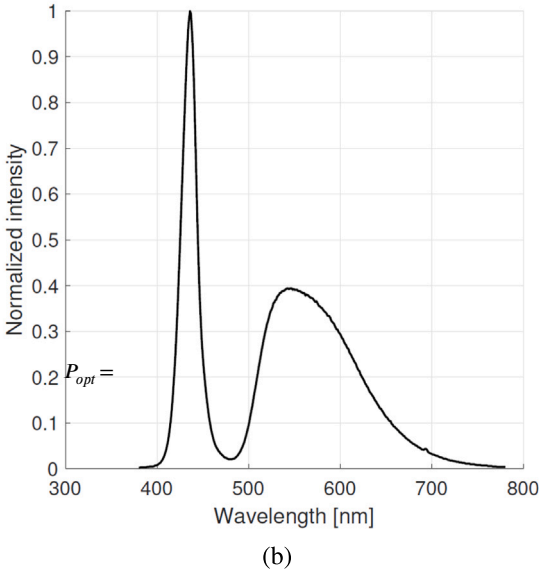

Fig. 9. High luminance LED optical characteristics: radiation pattern (a) and emission spectrum (b).

The luminous flux is required to proceed to LED emission model development. Since the light source is mounted on its cooling system, the use of an integrating sphere was not possible in our context. Moreover, the LED is composed of three chips. Thus, luminance measurement have been performed similarly to [24] to determine the luminous energy emitted per chip. For that, a radiometry calibrated camera LMK 5 equipped with a CCD sensor (resolution of 1380 × 1030 pixels) has been used. Knowing the luminance emitted per chip and since the light source is Lambertian, the luminous flux Φ_{opt} (lm) is computed as follows.

$$\Phi_{opt} = \pi L S \tag{12}$$

where S is the surface radiating in accordance to Lambert's law with a luminance L [25].

Based on the previous physical parameters, the LED efficiency E_L is computed according to Eq. (13).

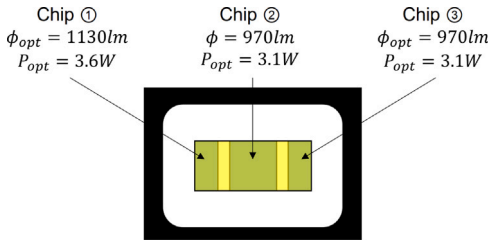

Fig. 10. Luminous flux and corresponding optical power emitted by each high luminance LED chip.

Table 3
Parameters of experimental set up.

Plate size	400 × 400 mm²
Plate thickness	1.5 mm
Distance LED - plate	35 mm
Distance plate - IR device	500 mm
Plate thermal conductivity	0.25 W/m K
Emissivity	0.9
Biot number	0.06<<1

$$E_L = \frac{K_m \int_0^\infty \Phi_e(\lambda) V(\lambda) d\lambda}{\int_0^\infty \Phi_e(\lambda) d\lambda} \tag{13}$$

where $K_m = 683 lm/W$ is the photopic luminous efficiency at a wavelength of 555 nm, $\Phi_e(\lambda)$ is the spectral radiant flux and $V(\lambda)$ is the photopic luminosity function that describes the average spectral sensitivity of the human visual perception of brightness [26].

The LED luminous efficiency is equal to 314lm/W. Thus, knowing the luminous flux, the optical power P_{opt} (W) emitted by each chip of the light source is determined by Eq. (14).

$$\frac{\Phi_{opt}}{E_L} \tag{14}$$

As shown on Fig. 10, luminance measurement reveals a non-uniform distribution of luminous flux (and consequently of optical power). This can modify the radiation behavior of the light source.

The previous experiments allowed to characterize the LED optical parameters, which will be used as input data in the emission model. Next section presents the experimental approach used for the simulation confrontation.

4. LED emission model validation using IR thermography

4.1. Experimental approach

To validate the LED emission model coupled to CFD simulation, an experimental set-up was designed, as shown in Fig. 11.

The principle of this experimentation takes up the general idea presented in previous work [27]. A PTFE plate is positioned in front of the LED mounted on its cooling system (composed of a heatsink, fan and heat pipe as presented in Section 2.1). The emissivity of the plate has been characterized using a spectrometer IRTF Vertex Bruker 70. Once the LED is switch on, the luminous energy is absorbed by the plate and increasing locally its temperature. Thus, an infrared camera FLIR SC325 is used to measure the temperature fields at the back face of the plate. Parameters of both experimentation and IR device are regrouped in Tables 3 and 4, respectively. By considering an exchange coefficient value of 10 W/m²K and the physical parameters of the plate (thickness of 1.5 mm and thermal conductivity of 0.25 W/mK), a Biot number of 0.06 is estimated: the experiment is well performed for a low Biot number, in order to avoid temperature gradient in the plate thickness.

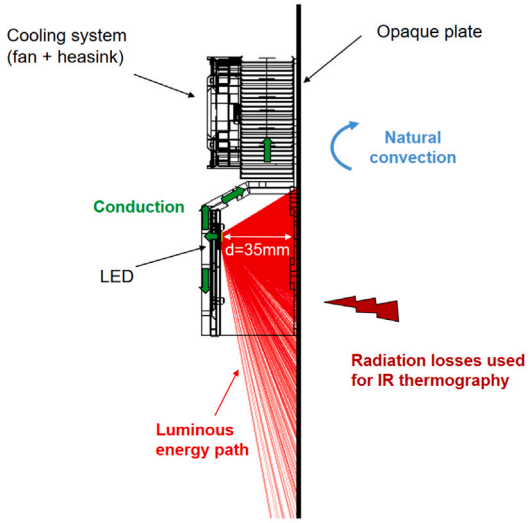

(a)

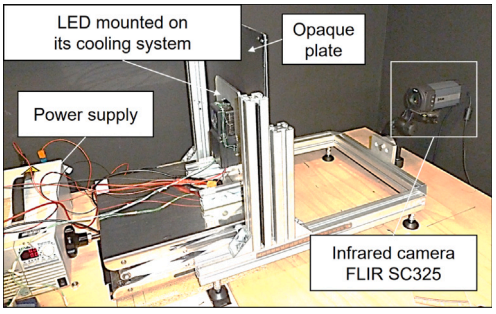

(b)

Fig. 11. Experimental set up: principle and description of physical phenomena (a) and experimental bench (b).

Table 4
Parameters of the IR camera FLIR SC325.

Resolution	320 × 256 pixels
Spectral band	[7.5–13] μm
Focal length	18 mm
Detector pitch	25 μm

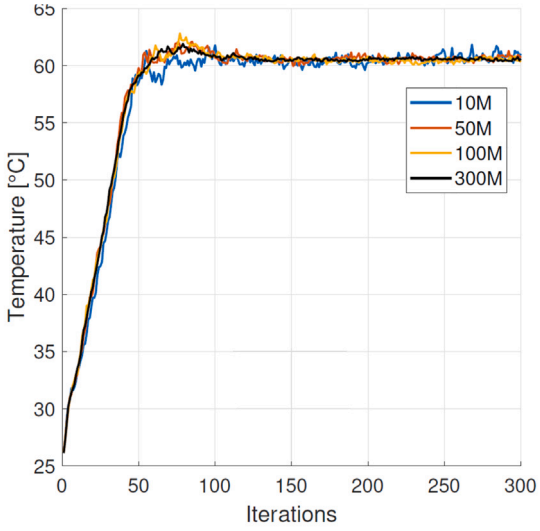

(a)

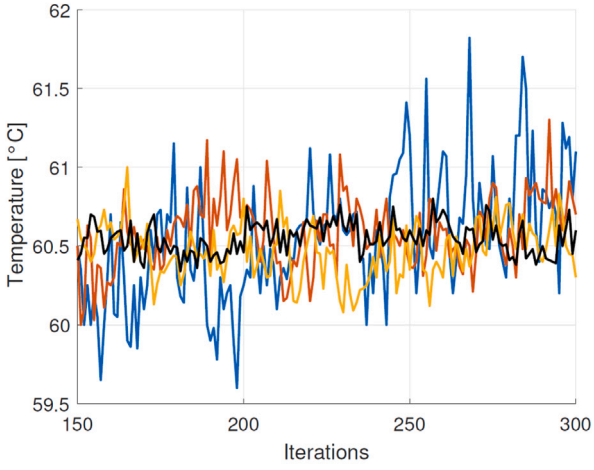

(b)

Fig. 12. Evolution of convergence versus number of rays (a) and zoom on the 150 last iterations (b).

As discussed in Section 2.2.2, 50 million rays is enough to ensure an error lower than 2.5% by comparing numerical results and analytical solution. However, this was defined based on a simple geometry. It is necessary to re-evaluate the sensitivity of number of rays in this more complex configuration. The computational time is less than seven hours with a workstation equipped with an Intel(R) Xeon (R) CPU ES-2630 v4 (40 CPUs @ 2.2 GHz) and 131 GB of RAM. Due to the workstation limitation, the numerical solution obtained for 300 million rays is considered as a reference in the following.

4.2. Rays number sensitivity

The sensitivity study starts with the analysis of calculation convergence. Fig. 12 proposes the visualization of maximum temperature versus iterations, obtained for 10, 50, 100 and 300 million rays. The number of iterations considered in the calculation is set to 300, to ensure the convergence. Focusing on the last 150 iterations (*i.e.* when the stabilization is reached), fluctuations are noticeable. They are induced by numerical noise, directly linked to the statistical approach of the RT method. The magnitude of fluctuation is rays-dependent: the lower the number of rays, the larger the fluctuations.

To quantify deviations from one calculation to another, the convergence study is deepened with the help of a statistical analysis. For that, the arithmetic mean $\overline{x}$, the standard deviation σ and the relative standard deviation RSD are used (Eqs. (15)–(17), resp.).

$$\overline{x} = \frac{1}{N}\sum_{i=1}^{N} x_i \tag{15}$$

$$\sigma = \sqrt{\frac{1}{N-1}\sum_{i=1}^{N}\left(x_i - \overline{x}\right)^2} \tag{16}$$

$$RSD = \left|\frac{\sigma}{\overline{x}}\right| \times 100 \tag{17}$$

Table 5 regroups the values of the quantities defined above. Even though the values of arithmetic mean are close, the standard deviation is lower as the number of rays increases. In addition, the RSD which measures the amount of relative dispersion shows that the temperature is more centered on the mean when the number of rays is higher. This is highlighted on histograms (Fig. 13). When 10 millions rays are traced, temperature values are uniformly distributed around the arithmetic mean. When the number of rays increases, temperature values are more

Table 5
Statistical analysis of the sensitivity of number of rays on the calculation convergence.

Rays	$\overline{x}$ [°C]	σ [°C]	RSD [%]
10M	60.56	0.41	0.6770
50M	60.60	0.23	0.3795
100M	60.48	0.17	0.2811
300M	60.56	0.10	0.1651

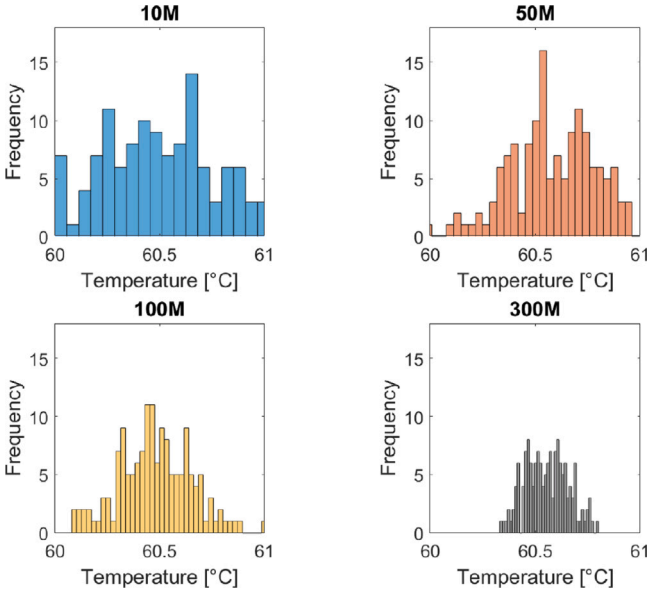

Fig. 13. Histograms obtained for each calculations.

centered on the arithmetic mean (as discussed above). According to the previous analyses, the computation convergence is reached when at least 50 million rays are traced. The second part of the sensitivity study is dedicated to the comparison of numerical temperature profiles at the back surface of plate.

Fig. 14 proposes the visualization of centered temperature profiles plotted in the x and y-directions. Fig. 15 displays the corresponding absolute deviation. As a reminder, the solution obtained for 300 million rays is considered as a reference (*cf.* Section 4.1). At the center of the plate, the number of rays does not have any significant influence on the shape of temperature profiles. Nevertheless, we can notice the presence of fluctuations obtained in -200 mm<x,y<-100 mm and 100 mm<x,y< 200 mm for both profiles. In addition, fluctuations are obtained in -75 mm<y<-25 mm, where a temperature step occurs. Far from the center of plate, irradiance level is low since less rays reach the low irradiance area (due to the stochastic process). Increasing the number of rays, the magnitude of fluctuations, and consequently the absolute deviation, decreases. The standard deviation value obtained for 300 million rays is too restrictive to define an acceptance criterion on temperature (*cf.* Table 5). Thus, the maximum acceptable deviation is taken equal to 0.5 °C, which is lower than 1% of the arithmetic mean for 300 million rays (δT=0.61 °C).

This acceptance criterion is illustrated by dashed lines on Fig. 15. According to horizontal temperature profiles and when only 10 million rays are traced, the most important deviations are obtained for |x|>100 mm, where the irradiance level on plate is the lowest. 50 million rays is sufficient to ensure a deviation lower than 0.5 °C. In addition, 100 million rays calculation induces a deviation greater than the criterion at the center of the plate. However, this does not have any significant influence on the shape of the entire profile. Regarding vertical profiles, the criterion is ensured even at the location of temperature step (*i.e.* -75 mm<y<-25 mm). According to the previous sensitivity study, 50 million rays is so sufficient to predict physical phenomena.

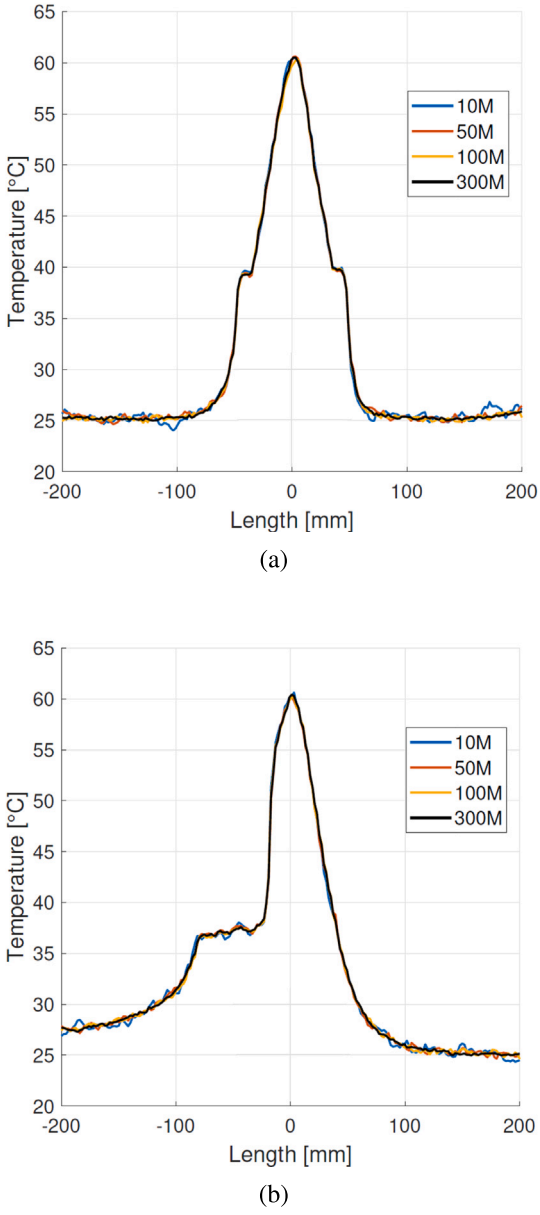

Fig. 14. Rays numbers sensitivity on horizontal (a) and vertical (b) temperature profiles.

Regarding computational costs, Fig. 16 shows the evolution of CPU time versus the number of rays. For 50 million of rays, CPU time is lower than two hours, which is quite low while the reference solution is obtained after six hours. Nevertheless, the CPU time depends not only on mesh size and number of rays [28,29] but also on physical phenomena numerically solved (*e.g.* radiation in semi-transparent material).

4.3. Validation of LED emission model

The LED emission model has been implemented in the commercial software FloEFD. Thermo-optic simulation consists of a coupling between CFD and radiation involving ray-tracing method (*cf.* Section 2). Thus, the final part of the study is dedicated to the comparison of numerical results with experimental data. Fig. 17 proposes the visualization of temperature fields obtained by measurement using the same IR camera as described in Table 4 and simulation on the back surface

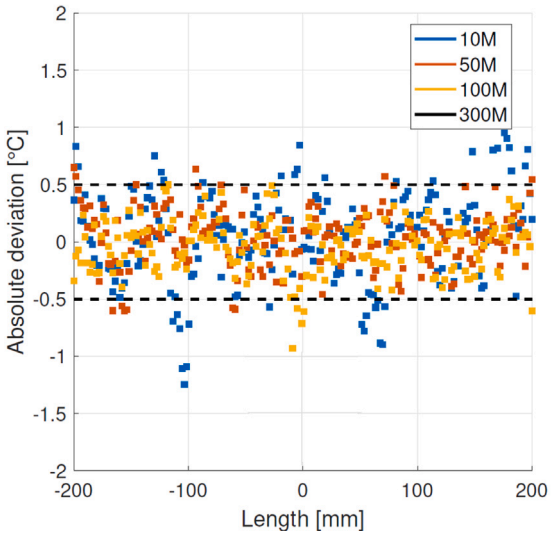

(a)

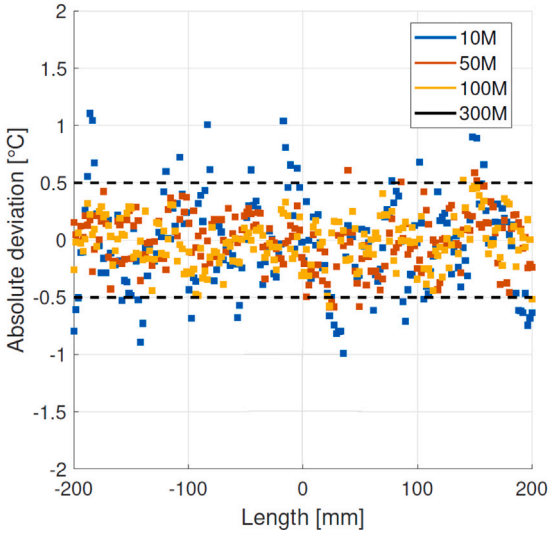

(b)

Fig. 15. Absolute deviation on horizontal (a) and vertical (b) temperature profiles.

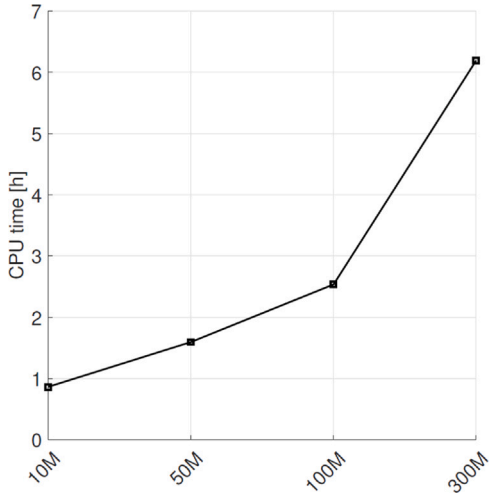

Fig. 16. Rays number versus CPU time.

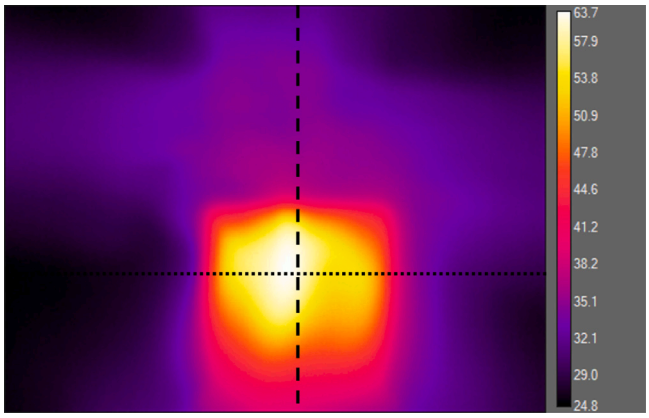

(a)

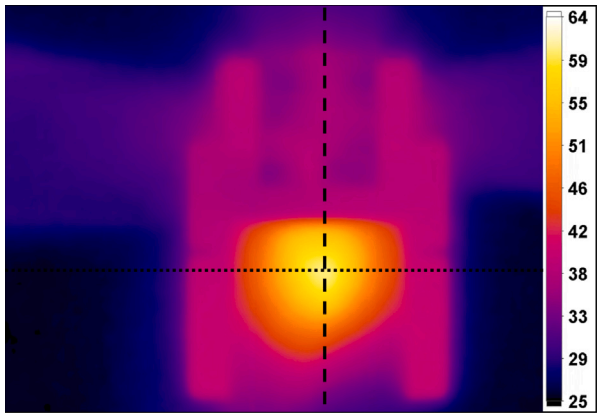

(b)

Fig. 17. Experimental (a) and numerical (b) temperature fields on back face of plate.

of plate. First, thermography reveals the presence of a hot region at the plate surface that is also predicted by simulation. The LED emits light that is absorbed by the plate: the plate is thus heated. In this region, an asymmetry on the temperature fields is detected and is directly linked to the non-uniform luminous flux emitted per high luminance LED chips (*cf.* Section 3). In addition, thermogram reveals the presence of three singularities represented by the isotherm areas (two in the horizontal direction and one the vertical direction, resp.).

To further analyze these phenomena, a visualization of convective fluxes obtained from CFD simulation is proposed, as shown on Fig. 18. The vertical singularities is a convective plume induced by natural convection occurring at the surface of the plate. Due to the asymmetry on the temperature fields on plate surface, this plume is also asymmetric. The two horizontal singularities are induced by the configuration of the LED cooling system: a fan blows air onto the heatsink. This results in an airflow generated by forced convection on each side of the heatsink. The three plumes detected by IR thermography are also predicted numerically. The simulation shows that the borders of the cooling system are clearly noticeable compared with experimental temperature fields. This can be explained by:

- A smoothness of temperature, directly induced by convective phenomena.
- A difference between the projection of a pixel in the object plane and the mesh size.
- A defocus aberration and/or an angular misalignment.
- A plate deformation induced by the temperature gradients.

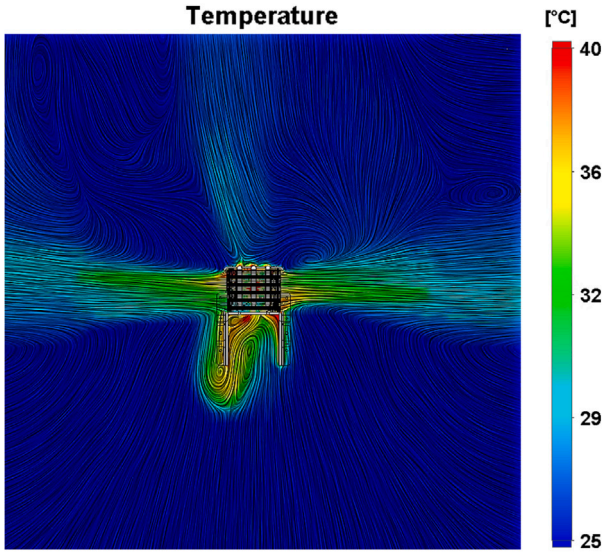

(a)

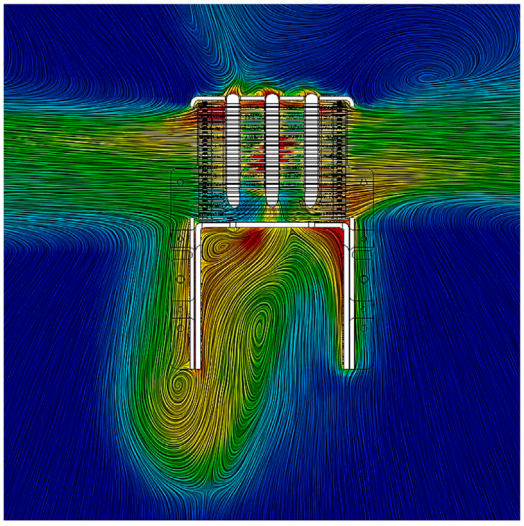

(b)

Fig. 18. Fluid flow analysis obtained on XY cut plane (a) and zoom on the interest area (b).

Fig. 19 proposes the visualization of centered horizontal and vertical profiles, represented respectively by dashed and dotted lines on Fig. 17. Both horizontal profiles follows the same trend. Nevertheless, the experimental temperature profile in the x-direction highlights an asymmetry not reproduced by computation. In addition, the maximum temperature predicted at the center of the plate is measured at a distance of 5 mm from the center. Secondly, simulation shows the presence of two discontinuities located in x=±35 mm. They are induced by the hot part of the cooling system and cannot be detected by thermography, due to convective phenomena: a smoothness occurs. Vertical temperature profiles follows the same trend, with notably a temperature step detected by thermography and also predicted by simulation. It is induced by the walls of the LED cooling system. Regarding maximum temperature, numerical and experimental values

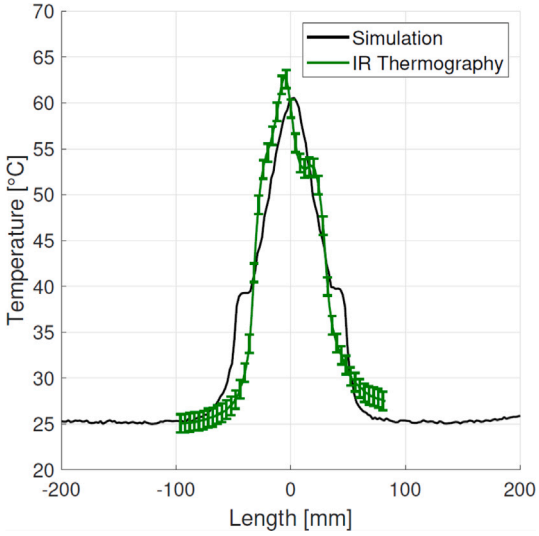

(a)

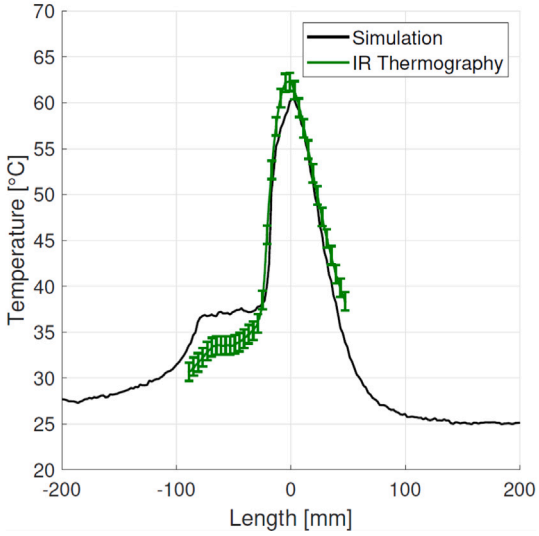

(b)

Fig. 19. Comparison of horizontal (a) and vertical (b) temperature profiles.

are respectively 60.5 °C and 62.8 °C. Based on the good agreement between numerical results and experimental data, the opto-thermal model of the high luminance LED is validated.

5. Conclusions

The main objective of this paper was to validate experimentally the opto-thermal simulation of a high luminance LED that emits a luminous energy up to 10 W. The simulation results were compared to IR thermography measurement. It can be noticed that:

- First, the validation of the Ray-Tracing approach was performed using a reference case for which an analytical solution exists. This allowed to study the influence of mesh sensitivity and number of rays sensitivities on the solution accuracy.
- Then, the full optical characterization of the component was performed for proceeding to the high luminance LED opto-thermal model development. Such a model was implemented in the commercial CFD software FloEFD™.

- Finally, the 3D opto-thermal simulation of the high luminance LED was confronted to experimental data obtained from IR thermography performed in a simple case (consisting of the illumination of a black plate subjected to the optical radiation emitted by the LED). This leads to the validation of the high luminance LED opto-thermal model with a deviation lower than 3 °C in the area of interest (*i.e.* on the maximum temperature of 62.8 °C).

Few deviations have also been highlighted between numerical results and experimental data. They can be attributed to: environmental effect (presence of another convection and/or radiation source), experimental effect (IR device focus, angular misalignment and plate deformation) and to CFD simulation that "idealizes" convective heat transfer. Moreover, since the LED architecture not yet stabilized, it can induce deviation as well (based on the non-uniformity of the optical power emitted per LED chips).

One main perspective might be to reproduce similar experiments on other LED light sources, to ensure to the robustness of the LED opto-thermal model. Moreover, it may be interesting to investigate the opto-thermal behavior of the full lighting system (that includes the LED mounted on its cooling system and the optical system projecting the luminous energy emitted by LED to the road). Another interesting topic will be to investigate the decrease of the calculation time, for example by using either high performance calculation (HPC) or calculation performed with graphic card.

Declaration of competing interest

The authors declare that they have no known competing financial interests or personal relationships that could have appeared to influence the work reported in this paper.

Data availability

The authors do not have permission to share data.

Acknowledgment

The authors would like to acknowledge Valeo Lighting System, France for having supported this work.

References

[1] S. Berlitz, C. Heider, LEDs in automotive lighting and signaling: a customer point of view, in: Manufacturing LEDs for Lighting and Displays, Vol. 6797, International Society for Optics and Photonics, 2007, 679704.
[2] M. Courcier, B. Reiss, V. Sanchez, New front lighting possibilities through high definition digital lighting, in: International Symposium on Automotive Lighting (Isal), Darmstadt, 2015.
[3] C. Lasance, A. Poppe, et al., Thermal Management for LED Applications, Springer, 2014.
[4] W. Moore, E. Donovan, C. Powers, Thermal analysis of automotive lamps using the ADINA-F coupled specular radiation and natural convection model, Comput. Struct. 72 (1–3) (1999) 17–30.
[5] A. Filipuzzi, O. Cotula, A. Pipino, F. Zanoletti, S. Paroni, Thermal behavior of bulb and LED based automotive rear lamps, in: 3rd European Automotive CFD Conference, Ansys, Inc. 2007, pp. 267–276.
[6] M. Dauphin, S. Albin, C. Roucoules, Y. Le Maoult, F. Schmidt, M. El-Hafi, Modélisation des échanges radiatifs dans un système d'éclairage automobile par la méthode de Monte-Carlo, in: SFT (Congrès Société Française de Thermique), 2013.
[7] S. Boztepe, O. De Almeida, R. Gilblas, Y. Le Maoult, F. Schmidt, C. Gerlach, A combined experimental and numerical approach for radiation heat transfer in semi-crystalline thermoplastics, Int. J. Therm. Sci. 142 (2019) 142–155.
[8] G. Barreto, P. Canhoto, M. Collares-Pereira, Three-dimensional CFD modelling and thermal performance analysis of porous volumetric receivers coupled to solar concentration systems, Appl. Energy 252 (2019) 113433.
[9] D. Ting, T. McGill Jr., Monte Carlo simulation of light-emitting diode light-extraction characteristics, Opt. Eng. 34 (12) (1995) 3545–3553.
[10] I. Moreno, C.-C. Sun, Modeling the radiation pattern of LEDs, Opt. Express 16 (3) (2008) 1808–1819.
[11] Z. Liu, K. Wang, X. Luo, S. Liu, Precise optical modeling of blue light-emitting diodes by Monte Carlo ray-tracing, Opt. Express 18 (9) (2010) 9398–9412.
[12] S. Lan, H. Wan, J. Zhao, S. Zhou, Light extraction analysis of AlGaInP based red and GaN based blue/green flip-fhip micro-LEDs using the Monte Carlo Ray Tracing method, Micromachines 10 (12) (2019) 860.
[13] J. Hertel, V. Martínez-Moll, R. Pujol-Nadal, F. Bonnín-Ripoll, State of the art of radiation-matter interaction models applied for the optical characterization of concentrating solar collectors, in: EuroSun Conference, Palma de Mallorca, Spain, Oct., 2016, pp. 12–14.
[14] M. Raypah, M. Dheepan, M. Devarajan, F. Sulaiman, Investigation on thermal characterization of low power SMD LED mounted on different substrate packages, Appl. Therm. Eng. 101 (2016) 19–29.
[15] A. Bejan, J. Lage, et al., The Prandtl number effect on the transition in natural convection along a vertical surface, J. Heat Transfer 112 (3) (1990) 787–790.
[16] Mentor Graphics, FloEFD for Catia V5, 2019, Technical Reference.
[17] M. Modest, Radiative Heat Transfer McGraw-Hill Inc., 1993.
[18] Mentor Graphics, Enhanced turbulence modeling in FloEFD, 2011.
[19] C. Rongier, R. Gilblas, Y. Le Maoult, S. Belkessam, F. Schmidt, Infrared thermography applied to the validation of thermal simulation of high luminance LED used in automotive front lighting, Infrared Phys. Technol. 120 (2022) 103980.
[20] Mentor Graphics, Advanced immersed boundary cartesian meshing technology in FloEFD, 2011.
[21] P. Planas Almazan, Accuracy of Monte Carlo ray-tracing thermal radiation calculations: A practical discussion, in: Sixth European Symposium on Space Environmental Control Systems, Vol. 400, 1997, p. 579.
[22] B. Cosson, F. Schmidt, Y. Le Maoult, M. Bordival, Infrared heating stage simulation of semi-transparent media (PET) using ray tracing method, Int. J. Mater. Form. 4 (1) (2011) 1–10.
[23] H. Leuenberger, R. Person, Compilation of Radiation Shape Factors for Cylindrical Assemblies, Technical Report, Electro Metallurgical Co Niagara Falls Ny, 1954.
[24] Y. Tyukhova, C. Waters, An assessment of high dynamic range luminance measurements with LED lighting, Leukos 10 (2) (2014) 87–99.
[25] H. Keitz, Light Calculations and Measurements: An Introduction to the System of Quantities and Units in Light-Technology and to Photometry, Macmillan International Higher Education, 1971.
[26] K. Sagawa, Y. Takahashi, Spectral luminous efficiency as a function of age, J. Opt. Soc. Amer. A 18 (11) (2001) 2659–2667.
[27] J. Mackie, O. De Almeida, F. Schmidt, K. Labastie, Modeling of IR lamps with coated reflector used in the slurry powder impregnation process of composite tapes, in: AIP Conference Proceedings, Vol. 2113, No. 1, AIP Publishing LLC, 2019, 130005.
[28] A. Wang, M. Modest, Spectral Monte Carlo models for nongray radiation analyses in inhomogeneous participating media, Int. J. Heat Mass Transfer 50 (19–20) (2007) 3877–3889.
[29] C. Fan, X. Xia, J. Qiu, C. Sun, mcrtFOAM: A mesh-agglomeration Monte Carlo ray-tracing solver for radiative transfer in gray semitransparent solids, Comput. Phys. Comm. 258 (2021) 107608.